2023

Thermal characterization of n-type silicon based on an electroacoustic analogy

N. Stanojevic, D. K. Markushev, S. M. Aleksić, D. S. Pantić, S. P. Galović, D. D. Markushev, J. Ordonez-Miranda

Published in:

Journal of Applied Physics

DOI:
10.1063/5.0152495

Document version:
Peer reviewed article (often known as postprint article)

Recommended citation:
Stanojevic, N., Markushev, D. K., Aleksić, S. M., Pantić, D. S., Galović, S. P., Markushev, D. D., & Ordonez-Miranda, J. (2023). Thermal characterization of n-type silicon based on an electro-acoustic analogy. Journal of Applied Physics, 133(24).

Thermal characterization of *n*-type silicon based on an electro-acoustic analogy

N. Stanojevic[1], D. K. Markushev[2], S.M. Aleksić[1*], D.S. Pantić[1],
S.P. Galović[3], D. D. Markushev[2], J. Ordonez-Miranda[4]

[1]*Faculty of Electronic Engineering, University of Niš, Aleksandra Medvedeva 14, 18000 Niš, Serbia*
[2]*Institute of Physics, University of Belgrade, Pregrevica 118, 11080 Belgrade-Zemun, Serbia*
[3]*Vinča Institute of Nuclear Sciences, P.O. Box 522, 11001 Belgrade, Serbia*
[4] *LIMMS, CNRS-IIS UMI 2820, The University of Tokyo, Tokyo, 153-8505, Japan.*

*Corresponding author: sanja.aleksic@elfak.ni.ac.rs

Abstract

Based on the analogy between *RC* filters and the thermoelastic component of the photoacoustic signal, the complex thermoelastic response of an open photoacoustic cell is described as a simple linear time-invariant system of a low-pass *RC* filter. This description is done by finding a linear relation between the thermoelastic cut-off frequency and the sample material thickness within the range of (10 – 1000) μm. Based on the theory of composite piston, we run numerical simulations of the proposed method for *n*-type silicon, described as either a surface or volume absorber. The theoretical predictions are experimentally validated by using an open photoacoustic cell set-up to record the signal of an 850-μm-thick *n*-type silicon wafer illuminated by a blue light source modulated with frequencies from 20 to 20 kHz. The obtained experimental results confirm the linear dependence of the thermoelastic cut-off frequency on the sample thickness, and therefore they lay the foundation of a new method for the thermal characterization of materials.

1. Introduction

Although photoacoustics is a powerful method that has been used for decades for the thermal characterization of solids and liquids [1-8], it also provides a platform for the development of new methods based not only on the analysis of its total signal, but also on its signal components for semiconductors [9-11]. By analyzing the frequency spectrum of the thermoelastic component of the photoacoustic signal generated by semiconductors, some research groups [12-14] recently showed that its patterns can be used to probe the influence of free carriers. Such analysis can be used in different areas, such as the design of heat sinks in electronic devices [15-17] and silicon membranes suitable for Micro Electromechanical Systems (MEMS) sensors [18-20].

The practice has shown that analog electrical networks are a suitable tool for representing systems and processes of diverse physical nature [21-23]. In particular, the linear time-invariant (LTI) systems are widely used to process signals modeling physical phenomena and implementing the desired effects on data. For instance, a simple LTI system made up of analog passive RC (resistor-capacitor) filters are commonly applied to pass data through and eliminate unwanted frequencies [24,25].

In this article, we show that a photoacoustic cell can be considered as a LTI system composed of an analog passive *RC* low-pass filter [26]. By finding the characteristic cut-off frequency (f_{TE}) of the thermoelastic component, this electroacoustic analogy is used to develop a new methodology for the thermal characterization of semiconductors. This methodology provides the cut-off frequency $f_{TE}(l)$ as a function of the sample thickness l, a unique curve for a given material. Numerical simulations of the frequency response of *n*-type silicon are performed to determine its characteristic curve in presence of surface or volume absorption, and without the influence of free carriers. Further, the proposed method is experimentally validated by using an open-cell photoacoustic setup to measure the photoacoustic signal of *n*-type silicon samples of different thicknesses. We selected this silicon sample because of its ability to act as both a surface (blue light, low absorption depth) or volume absorber (red light, high absorption depth), by changing the wavelength of the illumination light. This material behavior allows us treating the thermoelastic response of silicon in the simplest way (surface absorber) needed to establish the RC analogy.

2. Theoretical background

2.1. Fundamentals of linear time-invariant systems

Following the definition of a signal as the description of how one parameter varies with another, and the definition of the system as a process that maps an input signal to an output one, practice shows that the most useful systems fall into the LTI category [24,25]. This is the reason why the LTI systems are primary signal-processing tools, mostly represented as filters of different kinds. A LTI system has the following properties: homogeneity, additivity, and time invariance. Homogeneity means that a change in the input signal's amplitude results in a corresponding change in the output signal's amplitude, additivity means that the signals added at the input produce signals that are added to the output, and time invariance means that the system responds in the same way now or later [25].

Static linearity, sinusoidal fidelity, and commutativity are other useful properties of LTI systems [25], to understand the analogy between low-pass *RC* filters and photoacoustics. Static linearity defines how a LTI system reacts when the signals aren't changing (DC or static signals): the output is the input multiplied by a constant. Sinusoidal fidelity establishes that if the input to an LTI system is a sinusoidal wave, the output will also be a sinusoidal wave oscillating with the same frequency as the input. If two or more systems are combined in a cascade (the output of one system is the input to the next), and if each system is linear, then the overall combination will also be linear. The commutative property states that the order of the systems in the cascade can be rearranged without affecting the characteristics of the overall combination. As one of the most used ways of describing an LTI system is its frequency response, in this article, we are going to study this frequency in relation to a photoacoustic signal.

2.2. Analogue passive low-pass RC filters

Filters are electronic circuits that reject a band of frequencies and allows others to pass through. They alter a signal's amplitude and/or phase characteristics with respect to frequency in the way that the LTI system does. A filter circuit which consists of passive components such as resistors, capacitors, and inductors, is called a passive filter [27-29]. Considering that the operating frequency range of a filter is determined by the components used to build its circuit, a filter can be categorized based on the operating frequency of a particular circuit. The basic categories are low-

pass, high-pass, bend-pass, and bend-stop filters. Here, we will present fundamentals of the analogue passive low-pass *RC* filter (LPRCF). This filter provides a constant output (gain) from zero up to the cut-off frequency f_0, by attenuating all frequencies above f_0. The schemes of a LPRCF on time and frequency domains are shown in in Figures 1(a) and 1(b), respectively.

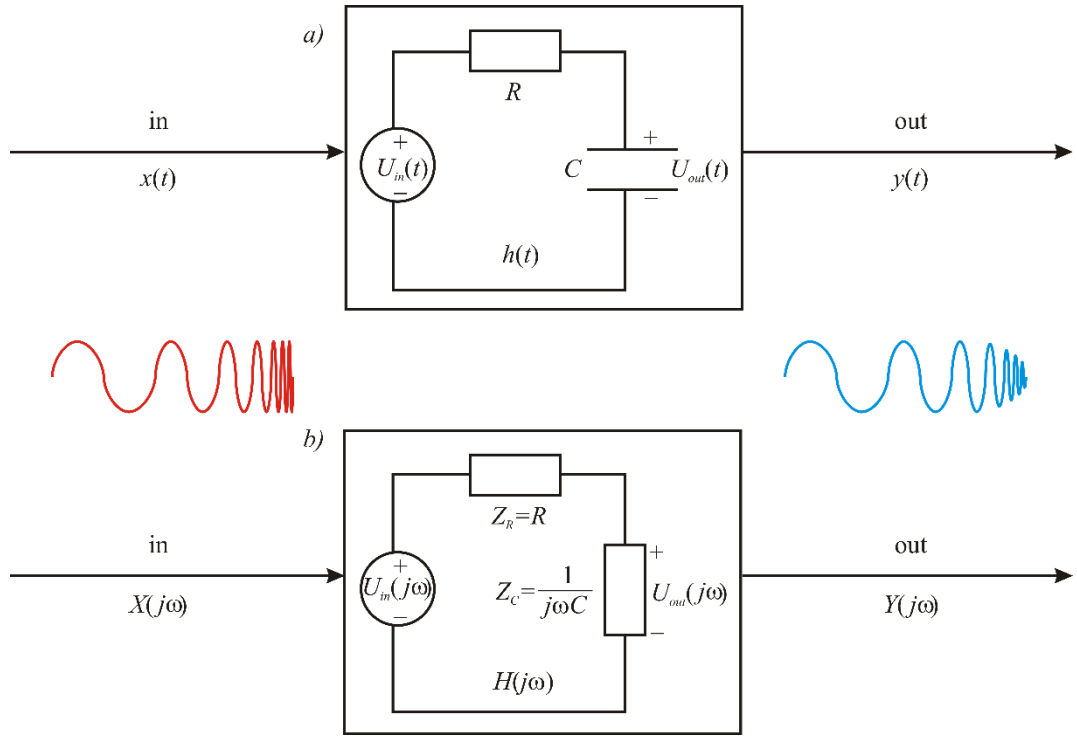

Figure 1. Typical LTI schemes of the low-pass *RC* filter on a) time and b) frequency domains. The red and blue lines stand for the usual sinusoidal input and output signals of the same frequencies.

Mathematically, a LPRCF is often described in terms of its transfer function $H(j\omega)$ (frequency response), which is given by the ratio of the Fourier transforms $Y(j\omega)$ and $X(j\omega)$ of its respective output and input signals, as follows:

$$H(j\omega)=\frac{Y(j\omega)}{X(j\omega)}=\frac{U_{out}(j\omega)}{U_{in}(j\omega)}=\frac{1}{1+j\dfrac{\omega}{\omega_0}}, \tag{1}$$

where j is the imaginary unit, $\omega=2\pi f$, f is the modulation frequency of the input signal, $\omega=2\pi f_0=1/RC$, with f_0 being the filter cut-off frequency, R the electrical resistance, C the capacitance, $U_{in}(j\omega)$ an input voltage (ideal voltage source), and $U_{out}(j\omega)$ an output voltage. As a complex quantity, the amplitude $|H(j\omega)|$ and phase φ of $H(j\omega)$ are given by:

$$\left|H\left(j\omega\right)\right| = \frac{1}{\sqrt{1+\left(\frac{\omega}{\omega_0}\right)^2}}, \tag{2}$$

and

$$\varphi = -\arctan\left(\frac{\omega}{\omega_0}\right). \tag{3}$$

To plot $\left|H\left(j\omega\right)\right|$ and φ for $0<\omega<\infty$, we obtain their values at the following characteristic points: 1) when $\omega\to 0$ then $\left|H\left(j\omega\right)\right|\to 1$ and $\varphi\to 0°$; 2) when $\omega\to\infty$ then $\left|H\left(j\omega\right)\right|\to 0$ and $\varphi\to 90°$; 3) when $\omega=\omega_0$ then $\left|H\left(j\omega\right)\right| = 1/\sqrt{2}$ and $\varphi = -45°$. According to Eqs. (2) and (3), and these characteristic points (black dots), the LPRCF frequency response is plotted and shown in Figure 2.

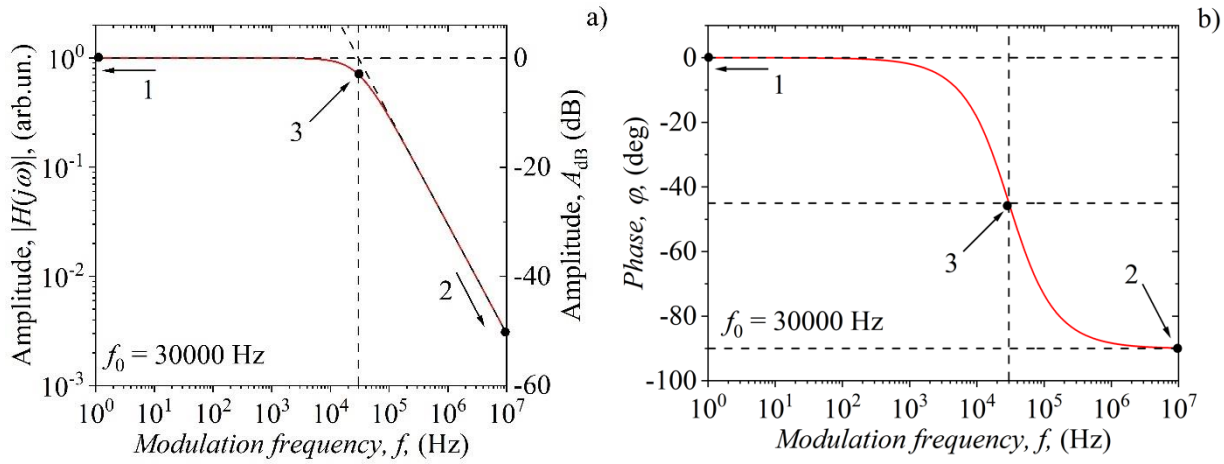

Figure 2. Frequency response of the a) amplitude and b) phase of a typical LPRCF. Calculations were done for f_0 = 30000 Hz and the amplitude in arbitrary units and decibels in (a).

To locate the crucial features of the amplitude and phase of the transfer function, we follow the standard practice to use Bode plots, semi-log plots of the amplitude (in decibels) and phase (in degrees) of a transfer function versus frequency. To obtain these Bode plots (Figure 2), we transformed the amplitude $\left|H\left(j\omega\right)\right|$ (Eq. (2)) into A_{dB} (in decibels) given by

$$A_{\mathrm{dB}} = 20\log\left|H\left(j\omega\right)\right|. \tag{4}$$

A_{dB} is shown in the right vertical axis in Figure 2(a) and contains the same information as the logarithmic plot of $\left|H\left(j\omega\right)\right|$, but it is much easier to construct and interpret. The phase φ, on the other hand, is shown in Figure 2(b) and its Bode plot remains the same.

2.3. Photoacoustic thermoelastic component

As it is well known, photoacoustics relies on the photoacoustic effect dealing with the generation of sound waves due to the modulated light absorption in a material [30-32]. Sound waves are usually detected by different kinds of sensors, usually microphones, in the form of the total photoacoustic signal – the time variation of the microphone electric output (voltage or current). Based on the theoretical model of the composite piston [33,34], the total photoacoustic signal $\delta p_{\text{total}}(j\omega)$ of the semiconductor, excited without the excess carriers influence, consists of two components: one generated by the thermal piston (thermo-diffusion component, $\delta p_{\text{TD}}(j\omega)$) and another one generated by the mechanical piston (thermoelastic component, $\delta p_{\text{TE}}(j\omega)$). Mathematically, the total photoacoustic semiconductor signal is a complex function composed of its two components, as follows:

$$\delta p_{\text{total}}(j\omega) = \delta p_{\text{TD}}(j\omega) + \delta p_{\text{TE}}(j\omega). \tag{5}$$

Being complex quantities, all components have amplitudes and phases. For our analysis, we will single out the thermoelastic component, $\delta p_{\text{TE}}(j\omega)$, of the semiconductor as the one whose frequency response, based on our experience, most closely matches the response of the low-pass *RC* filter - LPRCF.

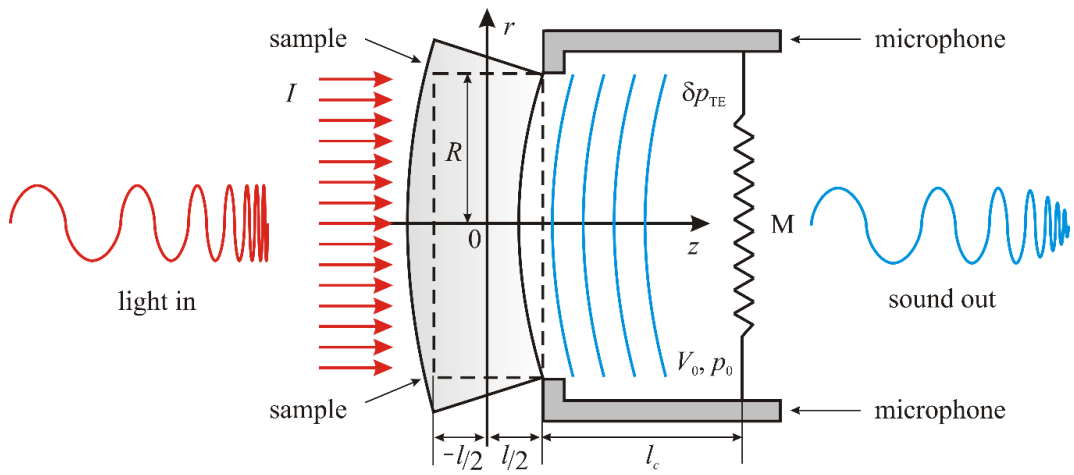

Figure 3. Scheme of a LTI for the photoacoustics thermoelastic frequency response. The red and blue lines represent the sinusoidal input (modulated light) and output (sound) signals oscillating at the same frequencies, as processed by an open photoacoustic cell.

A schematic representation of the most used set-up of photoacoustics, the so-called open cell set-up, is shown in Figure 3. The microphone is the detector of the photoacoustic cell having a length l_c, and volume V_0. Open cell fairly represents the photoacoustic set-up as an LTI system, with all its above-mentioned characteristics. The modulated light source (red lines and sinusoids) uniformly illuminates the front side of the semiconductor sample with a circular shape of thickness l and radius R (dashed sample lines). The energy of absorbed light on the illuminated surface and in the nearby volume is transformed into the thermal energy that is transferred through the sample

along the *z*-axes (1D transfer) changing the thermal state of the semiconductor. Such a change leads to different temperatures on the illuminated and non-illuminated side of the sample, which leads to its, so-called, thermoelastic bending (solid sample lines). The bending is periodic, consistently follows the rhythm of the light source, and periodically changes the air pressure in the immediate vicinity of the unilluminated side of the sample (mechanical piston). A change in air pressure creates sound, i.e., the thermoelastic component $\delta p_{\mathrm{TE}}\left(j\omega\right)$ of the photoacoustic signal is formed (blue curves). The sound propagates through the air (at atmospheric pressure p_0) and it is registered by the microphone membrane (M), having the typical frequency response (blue sinusoids) of the semiconductor illumination without the influence of free carriers (electrons and holes).

From a physics point of view, there are two classical different ways to describe the temperature distribution of a semiconductor during its illumination (Figure 1): 1) surface absorption and 2) volume absorption, both without the excess carrier influence. Avoiding deeper analysis and derivation of the main temperature distribution equations, we will only present the final expressions and the underlying ideas about the new methods of thermal characterization based on electro-acoustic analogies between *RC* filters and photoacoustics. Based on the model of the composite piston [33,34] and the theory of thermoelastic bending [35,36], the thermoelastic component $\delta p_{\mathrm{TE}}\left(j\omega\right)_{\mathrm{i}}$ of the photoacoustic signal is given by:

$$\delta p_{\mathrm{TE}}\left(j\omega\right)_{\mathrm{i}} = 3\pi \frac{\gamma_g p_0 \alpha_T R^4}{l^3 V_0} \int_{-l/2}^{l/2} z T_{\mathrm{i}}\left(z\right) dz \,, \tag{6}$$

where $T_i\,(z)$ is the temperature distribution within the sample in the case of surface (i = s) or volume (i = v) absorber, p_0 is the air pressure in the cell volume V_0, γ_{g} is the ratio of the heat capacities of the intracell air, and α_{T} is the coefficient of thermal linear expansion of the sample.

2.4. Surface absorber without excess carrier influence

In this section, we will show how electro-acoustic analogies can be established between the frequency response of the thermoelastic component of the photoacoustic signal and the low-pass *RC* filter. In the case of *n*-type semiconductor surface absorption without excess carrier influence, solving the parabolic heat conduction equation (PHCE), the temperature distribution $T_{\mathrm{s}}\left(z\right)$ within the illuminated semiconductor (1D heat transport along the *z*-axes and geometry presented in Figure 1) can be written by a simple expression [37,38]:

$$T_{\mathrm{s}}\left(z\right) = \frac{I_0}{k\sigma} \frac{\cosh\left[\sigma\left(l/2 - z\right)\right]}{\sinh\left(\sigma l\right)} \,, \tag{7}$$

where I_0 is the amplitude of the incident light intensity I, $\sigma = \left(1+j\right)\mu^{-1}$ is the complex wave vector of heat diffusion, $\mu = \sqrt{2D_T/\omega}$ is the thermal diffusion length, $\omega = 2\pi f$ and f is the light source modulation frequency, D_{T} is the thermal diffusivity, and k is the thermal conductivity of the sample.

Solving the integral in Eq. (6) with $T_s(z)$ (Eq. (7)) yields a simple analytical expression for the thermoelastic component $\delta p_{TE}(j\omega)_s$ [37,38]:

$$\delta p_{TE}(j\omega)_s = 3\pi \frac{I_0 \gamma_g p_0 \alpha_T R^4}{2kV_0(\sigma l)^2} \left\{ \frac{\tanh(\sigma l/2)}{\sigma l/2} - 1 \right\}, \quad (8)$$

which can be easily analyzed in detail. The amplitude $A_{TE}(f)_s$ and phase $\varphi_{TE}(f)_s$ of $\delta p_{TE}(j\omega)_s$ (Eq. (8)) as a function of light source modulation frequency f are numerically obtained using MATLAB and presented in Figure 4 (blue solid lines), in the case of $l = 40$ μm thick n-type silicon (Si) sample with basic parameters given in Table I. The resulting $\delta p_{TE}(j\omega)_s$ responses are very similar to the $|H(j\omega)|$ (Eq. (2)) and φ (Eq. (3)) responses of the RC filter (Figure 3). Based on such obvious similarity, the RC fit is performed on amplitude $A_{TE}(f)_s$ and phase $\varphi_{TE}(f)_s$ (Eqs. (2) & (3) respectively, Figure 4, red dashed lines) which reveals that $\delta p_{TE}(j\omega)_s$ has the cut-off frequency $f_{TEs} = (9.1 \pm 0.1) \times 10^4$ Hz. Small discrepancies were observed between $\delta p_{TE}(j\omega)_s$ and RC fit at higher frequencies, roughly $f_{cr} > 2 \times 10^5$ Hz, both in amplitude and phase.

Table I. Si n-type sample parameters used in Eq. (16).

Thermal conductivity, k (W/mK)	150
Heat capacity, C (J/kgK)	715
Density, ρ (kg/m^3)	2329
Thermal diffusivity, D_T (mm^2/s)	90.0
Linear thermal expansion, α_T / (10^{-6} 1/K)	2.60

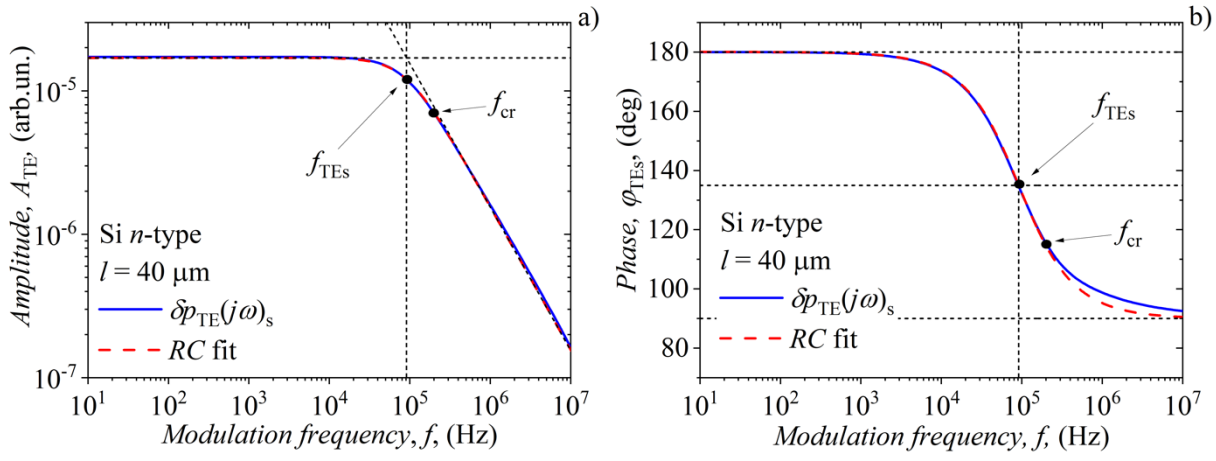

Figure 4. Frequency response of the a) amplitude and b) phase of $\delta p_{TE}(j\omega)_s$ (black solid lines) for a n-type Si sample of thickness $l = 40$ μm, together with their RC fit (red dashed lines).

The question arises here whether the obtained fitting results have justification and meaning, knowing that our photoacoustic system is a system described by partial differential equations, so-called distributed parameter system (DPS), while *RC* filters are typical representatives of systems described by ordinary differential equations, so-called lumped-parameter systems (LPS).

Without going into the details, the justification and meaning of obtained results are as follows: in a previous article [26], the condition that should be met to make the photothermal induced temperature variations of a solid sample analogous to the voltage variations of the electric network with passive linear elements is presented. Temperature variations are calculated using the hyperbolic heat conduction equation (HHCE) if the relaxation time τ of thermal processes in the medium exists $(\tau \neq 0)$. It was found that HHCE based photothermal (photoacoustic) system (DPS), can be represented as linear passive electrical network (LPS) under the certain conditions $|\sigma| l < \sqrt{6}$ ([26], see Appendix I) where σ is defined by *RLC* filter. Taking our PHCE case $(\tau \to 0)$ these conditions remain, but σ is reduced to *RC* filter. In addition, our photoacoustic thermoelastic system can be described only with resistors and capacitors ([26], see Appendix I). Considering description of σ by passive electrical elements (resistor, capacitor, coil), the similar condition for modeling of TE component by passive linear electrical network can be obtained: $|\sigma| l / 2 < \sqrt{6}$, (see Appendix I). For $\tau = 0$ (our case) this electrical network becomes *RC* filter (see Appendix I).

The stated condition can be adapted to our analysis (Figure 5), where for the range of Si sample thicknesses from 10 to 1000 microns, the range of critical modulation frequencies $4\times10^2 < f_{\text{cr}} < 4\times10^6$ Hz is determined (DPS - LPS approximation). When $l = 40$ μm (Figure 4), the photoacoustic system thermoelastic response can be described only by resistors and capacitors - a low-pass *RC* filter – LPRCF, at frequencies $f_{\text{cr}} < 2\times10^5$ Hz.

Last results show the possibility to develop an electric network – *RC* low pass filter (Figure 1) that will be the analog of the photoacoustic system under consideration (Figure 3). More precisely, the illuminated sample is modeled by LPRCF, where the values of voltages and electric currents in this filter are analog to the values of temperature distribution and heat flux at the respective points of the sample. The resistor corresponds to the reciprocal value of the sample thermal conductivity, and the capacitor corresponds to the sample thermal capacity.

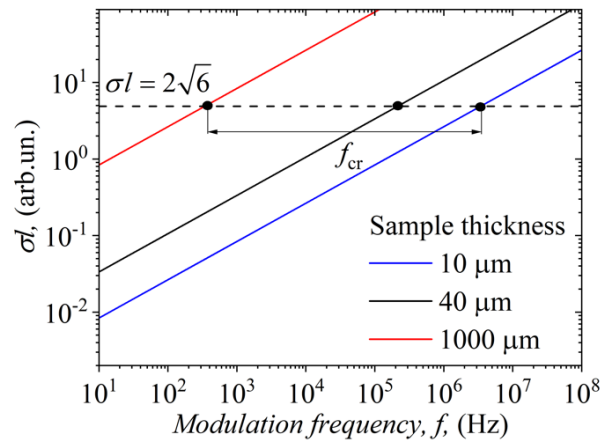

Figure 5. The values of σl as a function of modulation frequencies, *f*, in the case of *n*-type silicon (Table I) different thicknesses, and corresponding range of critical frequencies, f_{cr}, (between red and blue solid lines).

2.5. Volume absorber without excess carrier influence

In the case of *n*-type semiconductor volume absorption without free carrier influence, under the same excitation condition as in surface absorber case, the temperature distribution $T_{\mathrm{v}}(z)$ (1D case) within the semiconductor can be written as [37,38]:

$$T_{\mathrm{v}}(z)=\frac{I_0}{k\sigma}\frac{\beta^2}{\beta^2-\sigma^2}\left\{\frac{\cosh\left[\sigma\left(l/2-z\right)\right]-e^{-\beta l}\cosh\left(\sigma\left(l/2+z\right)\right)}{\sinh\left(\sigma l\right)}-\frac{\sigma}{\beta}e^{-\beta\left(l/2+z\right)}\right\}, \qquad (9)$$

Here, β is the absorption coefficient of the sample. Solving the integral in Eq. (6) with $T_{\mathrm{v}}(z)$ (Eq. (11)) yields a slightly more complicated analytical expression for the thermoelastic component $\delta p_{\mathrm{TE}}(j\omega)_{\mathrm{v}}$ [37,38]:

$$\delta p_{\mathrm{TE}}(j\omega)_{\mathrm{v}}=3\pi\frac{I_0\gamma_{\mathrm{g}}p_0\alpha_T R^4}{2kV_0\left(\sigma l\right)^2}\frac{\beta^2}{\beta^2-\sigma^2}\left\{\left(1+e^{-\beta l}\right)\left[\frac{\tanh\left(\sigma l/2\right)}{\sigma l/2}-1\right]-\left(\frac{\sigma}{\beta}\right)^2\frac{C}{\beta l}\right\}, \qquad (10)$$

where $C=2-\beta l-\left(2+\beta l\right)e^{-\beta l}$. The amplitude $A_{\mathrm{TE}}(f)_{\mathrm{v}}$ and phase $\varphi_{\mathrm{TE}}(f)_{\mathrm{v}}$ of $\delta p_{\mathrm{TE}}(j\omega)_{\mathrm{v}}$ as a function of light source modulation frequency *f* are presented in Figure 6 (blue solid lines), in the case of $l=40\mu\mathrm{m}$ thick n-type Si sample with basic parameters given in Table I, adding $\beta=2{,}41\times10^{6}\,\mathrm{m}^{-1}$ and excess carrier lifetime $\tau\approx10^{-9}\mathrm{s}$ (ultrafast recombination – no excess carriers influence).

It is obvious that $A_{\mathrm{TE}}(f)_{\mathrm{v}}$ and phase $\varphi_{\mathrm{TE}}(f)_{\mathrm{v}}$ of $\delta p_{\mathrm{TE}}(j\omega)_{\mathrm{v}}$ are the same as in the surface absorber case ($\beta l\to\infty$). It means that the *RC* fit (Eqs. (2) & (3), Figure 6, red dashed line) reveals the same value of $f_{\mathrm{TEv}}=f_{\mathrm{TEs}}=\left(9.1\pm0.1\right)\times10^{4}$ Hz. Also, it reveals the same values of f_{cr} as in the surface absorption case at $l=40\mu\mathrm{m}$ ($f_{\mathrm{cr}}<2\times10^{5}\mathrm{Hz}$) and in the whole investigated range of thicknesses $\left(10^{3}\ \mathrm{Hz}<f_{\mathrm{cr}}<10^{7}\ \mathrm{Hz}\right)$.

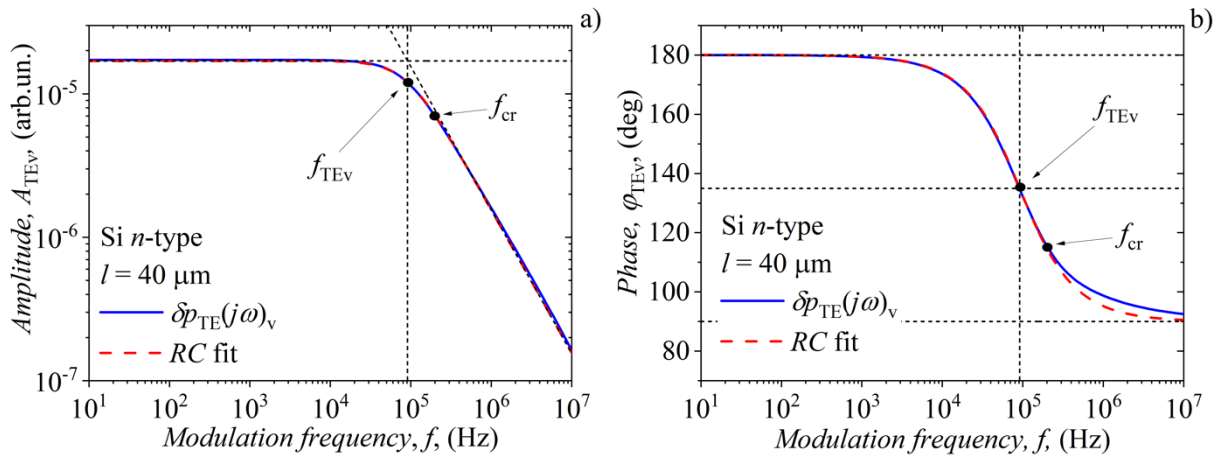

Figure 6. Typical $\delta p_{TE}(j\omega)_v$ a) amplitude and b) phase frequency responses (black solid lines) in the case of Si n-type sample having the thickness, $l = 40$ μm, together with their *RC* fit (red dashed lines).

3. New method for material characterization

In the previous paragraphs (section 2) we found the essential characteristics of our thermoelastic photoacoustic system: f_{TE}, f_{cr} (Figures 4,6), and dependence of f_{cr} on the sample thickness, l (Figure 5). In this paragraph, we will find another essential characteristic of our system, which is the dependence of f_{TEs} on l. This dependence is the basis of establishing a new material characterization method that connects the external parameters (f_{TEs}, l) that can be changed in the experiment, with the internal essential one (thermal diffusivity, D_T), a natural material characteristic. It can be found from $\sigma l / 2$ value in square brackets of Eq. (8) when $f = f_{TEs}$. In this case, one can write:

$$\frac{|\sigma| l}{2} = m, \tag{11}$$

or

$$f_{TEs} = \frac{2}{\pi} \frac{D_T}{l^2} m^2, \tag{12}$$

considering that $|\sigma| = \sqrt{\omega / D_T}$, $\omega = \omega_{TEs} = 2\pi f_{TEs}$, and $\sqrt{2} \le m < \sqrt{6}$ (see Appendix I) [26].

Applying the identical procedure as in Figure 6, f_{TEs} values can be found from $\delta p_{TE}(j\omega)_s$ (Eq. (8)), for a wide range of silicon sample thicknesses (from 10-1000 μm, Figure 7, Table II), with the same characteristics as it was given in Table I. Thicknesses are taken from $l_{min} = 10$ to 100 μm in steps of 10 μm, and from 100 to $l_{max} = 1000$ μm in steps of 100 μm.

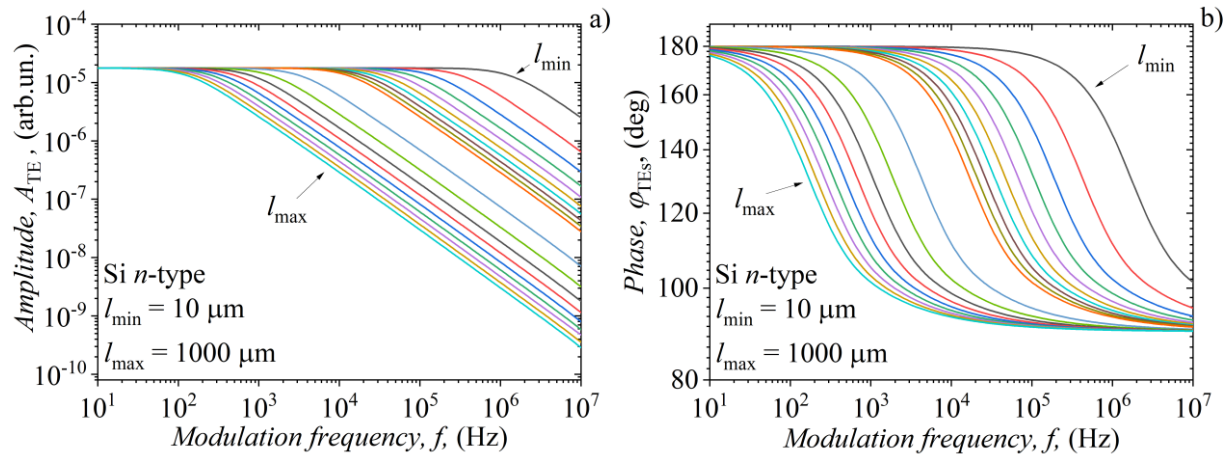

Figure 7. Frequency response of the a) amplitude and b) phase of $\delta p_{TE}(j\omega)_s$ for a *n*-type Si sample. Calculations were done for a sample thickness in the range (10-1000) μm, which is used to find f_{TEs} applying a *RC* fit (Eqs. (2) and (3)).

Table II. Cut-off frequency f_{TEs} determined by fitting for a *n*-type Si semiconductor of different thicknesses.

Sample thickness l / ($\times 10^{-6}$ m)	Cut-off frequency f_{TEs} / (Hz)
10	1467250
20	352064.0
30	150994.8
40	91465.38
50	58578.48
60	40865.79
70	28097.52
80	21687.13
90	17231.35
100	14013.44
200	3475.289
300	1578.390
400	871.7279
500	558.1317
600	387.6765
700	284.8613
800	217.3823
900	172.3485
1000	139.6089

Using the results presented in Table II, one can plot the dependence of f_{TEs} on the thickness of the sample, *l*, in a log-log scale (Figure 8). By fitting these results with Eq. (12), the value of $m = (1.513 \pm 0.002)$ is obtained. This result, in a general sense, represents a reference curve for a certain material (*n*-type Si in our case with parameter D_T from Table I) and can be used as a calibration curve within the framework of material characterization. In other words, a new method for material characterization (not only semiconductors), based on the analysis of the $\delta p_{TE}(j\omega)_s$

frequency response and its f_{TEs} dependence on the thickness of the sample, can be established. Such a methodology can be advantageous when it comes to the development of non-destructive methods of material characterization, investigation of semiconductor wafers as substrates for thin film analysis, as well as the role of photogenerated excess carriers both at surfaces and in bulk [39-43].

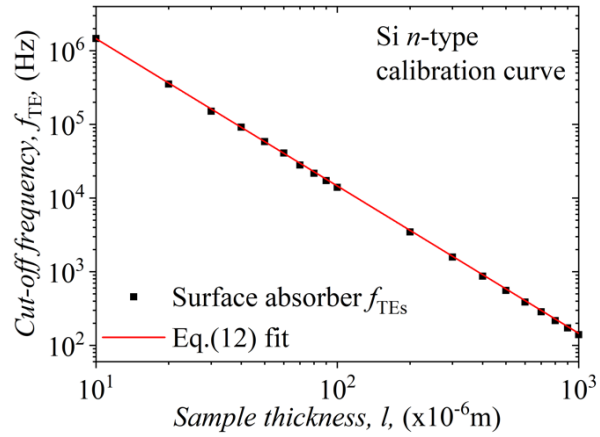

Figure 8. The calibration curve of *n*-type Si, showing the cut-off frequencies f_{TEs} of $\delta p_{TE}(j\omega)_s$ as a function of the sample thickness (Table II).

4. Experimental confirmation

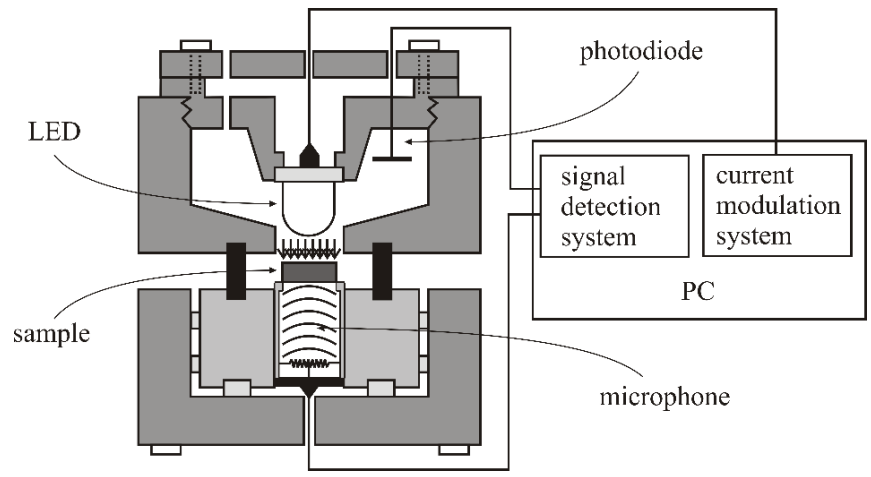

Figure 9. Scheme of the open-cell photoacoustic set-up.

To experimentally confirm the validity of the calibration method described in the previous section (section 3), let us use the measurement results of a circular *n*-type silicon wafer with a radius of $R = 3$ mm and a thickness of $l = 850$ μm. Measurements were made by the open-cell photoacoustic set-up (Figure 9), explained in detail somewhere else [12,13], with a blue LED light

source (450 nm), and corresponding wafer absorption coefficient $\beta = 2,41\times10^{6}\,\mathrm{m}^{-1}$ ($\beta l >> 1$, surface absorption) and excess carriers relaxation time, $\tau \approx 10^{-6}$ s, insufficient for their influence on photoacoustic signal (and it's components) in the 20 Hz to 20 kHz modulation frequency f range.

The obtained measured signal $S(j\omega)_s$ - its amplitude A and phase φ (red asterisks, Figure 9, a, b) are cleaned from the influence of the experimental instruments in the low- ($H_e(j\omega)$) and high-frequency ($H_a(j\omega)$) regions, in order to obtain the "true" signal $\delta p_{total}(j\omega)_s$ amplitudes and phases (solid blue lines, Figures 10 (a) and 10 (b)), the signal originating directly from the illuminated sample [13,44] (see Appendix II).

The obtained $\delta p_{total}(j\omega)_s$ is fitted using the composite piston model (solid blue, Figures 10 (c) and 10 (d)). Besides the basic sample parameters (matching those from Table I), such a fitting procedure leads to the signal components: $\delta p_{TD}(j\omega)_s$ from the thermal (dashed red), and $\delta p_{TE}(j\omega)_s$ from the mechanical (dashed blue) piston [13,33,34,44].

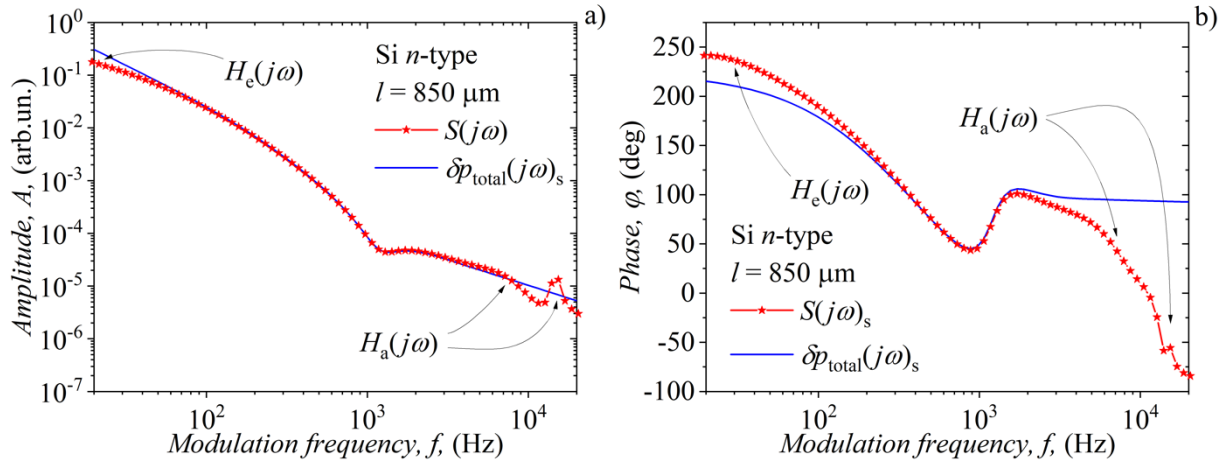

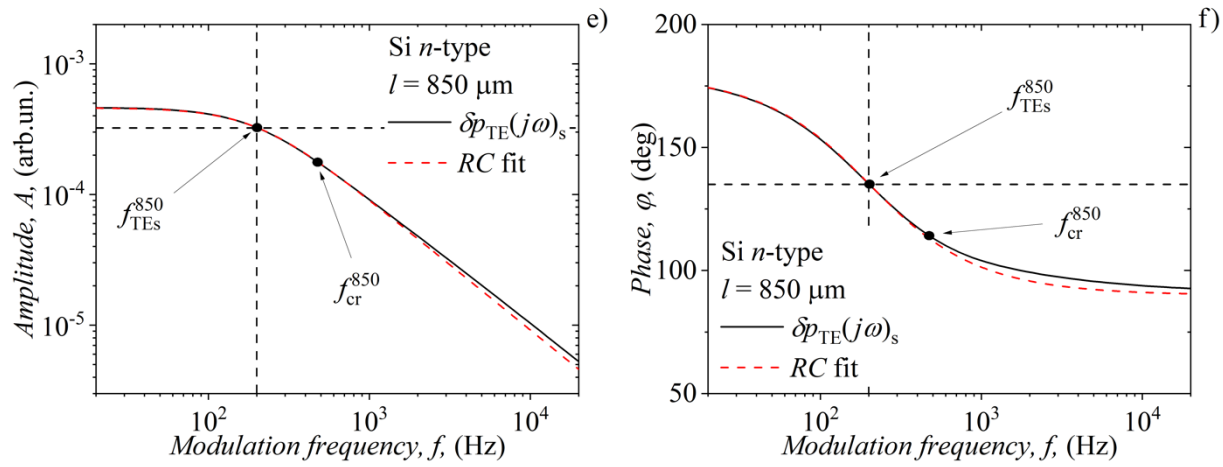

Figure 10. Measured photoacoustic signal $S(j\omega)_s$ of a *n*-type Si sample together with its "true" signal $\delta p(j\omega)_s$. a) amplitude *A* and b) phase φ are plotted together with the $\delta p(j\omega)_s$ components in c,d) $\delta p_{TD}(j\omega)_s$ and $\delta p_{TE}(j\omega)_s$, as a function of modulated frequency *f*. *RC* fits (Eq. (2) & (3)) are depicted on e) amplitude *A* and f) phase φ together with characteristic frequencies f_{TE}^{850} and f_{cr}^{850}.

Singling out $\delta p_{TE}(j\omega)_s$ (solid black, Figures 10 (e) and 10 (f)), it is clear that the analogy with *RC* circuits can be applied to this component, i.e. its amplitudes and phases can be fitted with equations (2) and (3), respectively (red dashed). The results of that fitting give the value of cut-off frequency $f_{TEs}^{850} = (200 \pm 10)$ Hz and $f_{cr}^{850} = (480 \pm 20)$ Hz. The value of f_{TEs}^{850} matches to the Si *n*-type calibration curve (Figure 11), and $f < f_{cr}^{850}$ defines the frequency range where *RC* fit of $\delta p_{TE}(j\omega)_s$ is fully applicable.

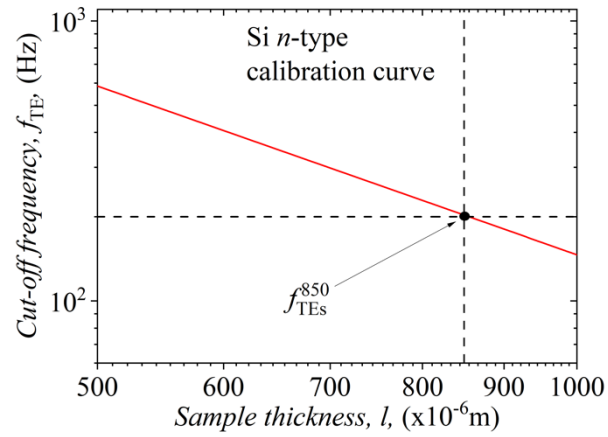

Figure 11. Cut-off frequency f_{TE}^{850} experimentally obtained (black dot) for a 850-µm-thick circular silicon wafer compared to the *n*-type silicon calibration curve (solid red line) predicted by theory (Figure 8).

The results obtained from the experimental data confirm the applicability of the new method aimed at the thermal characterization of *n*-type silicon based on electro-acoustic analogies between passive low-pass *RC* filters and thermoelastic components of the photoacoustic signals.

5. Conclusions

We have demonstrated that the thermoelastic response of n-type silicon recorded via an open photoacoustic cell can be described as a simple linear time-invariant system made up of a passive *RC* filter. This analogy is driven by the linear relation between the silicon sample thickness and the modulation frequency of its thermal excitation. For both surface and volume excitations without the influence of free carriers, we have obtained the values of the critical frequencies, below which the analogy between the photoacoustic (temperature, heat flux, thermal conductivity, heat capacity) and electrical (voltage, current, resistance, capacitance) quantities is complete. Based on the proposed analogy, the frequency spectrum of the amplitude and phase of the thermoelastic component of the silicon photoacoustic signal has been analyzed like a passive low-pass *RC* filter to determine the characteristic thermoelastic cut-off frequencies. By correlating the obtained cut-off frequencies with the thickness of the examined *n*-type silicon, we have determined that its linear calibration curve is driven by the thermal diffusivity. Such linearity has been experimentally validated using an open cell set-up to measure the photoacoustic response of the 850-μm-thick silicon wafer excited with a blue light source within the 20 Hz – 20 kHz modulation frequency range. The proposed method is thus expected to be useful for the thermal characterization of materials.

Acknowledgement

The authors acknowledge the financial support provided by the Institute of Physics Belgrade, through the grant n° 660-01-00015/69, of the Ministry of Science, Technological Development, and Innovations of the Republic of Serbia.

References

[1] S Engel, C Wenisch, F A Müller and S Gräf, A new photoacoustic method based on the modulation of the light induced absorption coefficient, *Measurement Science and Technology*, **27**, (4), (2016), 045202, http://dx.doi.org/10.1088/0957-0233/27/4/045202

[2] Aloisi Somer, Anderson Gonçalves, Thiago V Moreno, Gerson Kniphoff da Cruz, Mauro L Baesso, Nelson G C Astrath and Andressa Novatski, Photoacoustic signal with two heating sources: theoretical predictions and experimental results for the open photoacoustic cell technique, *Measurement Science and Technology*, **31**, (7), (2020), 075202, http://dx.doi.org/10.1088/1361-6501/ab786a

[3] D. Gasca-Figueroa, G. Gutiérrez-Juárez, F.J. García-Rodríguez, L. Polo-Parada, A. Pérez-Pacheco, M.G. Bravo-Sánchez, Direct measurement of solids thermal effusivity by cw photoacoustic technique, *Results in Physics*, **42** (2022), 105986, https://doi.org/10.1016/j.rinp.2022.105986

[4] Sarkar M, Kumar K., Fabrication of photoacoustic cell and thermal diffusivity measurement of coal carbon black using it, *Materials Today: Proccedings* **52**, (3), (2022), 1812-1816, https://doi.org/10.1016/j.matpr.2021.11.467.

[5] A. Somer, S. Galovic, E.K. Lenzi, A. Novatski, K. Djordjevic, Temperature profile and thermal piston component of photoacoustic response calculated by the fractional dual-phase-lag heat conduction theory, *International Journal of Heat and Mass Transfer*, **203**, (2023), 123801, https://doi.org/10.1016/j.ijheatmasstransfer.2022.123801
[6] Aloisi Somer, Andressa Novatski, Ervin Kaminski Lenzi, Theoretical predictions for photoacoustic signal: Fractionary thermal diffusion with modulated light absorption source, *European Physical Journal Plus*, **134** (12), (2019), https://doi.org/10.1140/epjp/i2019-12900-y
[7] Dmitry S. Volkov, Olga B. Rogova, Mikhail A. Proskurnin, Photoacoustic and photothermal methods in spectroscopy and characterization of soils and soil organic matter, *Photoacoustics*, **17** (2020) 100151, https://doi.org/10.1016/j.pacs.2019.100151
[8] Mykola Isaiev, Gauhar Mussabek, Pavlo Lishchuk, Kateryna Dubyk, Nazym Zhylkybayeva, Gulmira Yar-Mukhamedova, David Lacroix and Vladimir Lysenko, Application of the Photoacoustic Approach in the Characterization of Nanostructured Materials, *Nanomaterials*, **12** (4), (2022), 708, https://doi.org/10.3390/nano12040708
[9] Zelewski, S.J., Kudrawiec, R. Photoacoustic and modulated reflectance studies of indirect and direct band gap in van der Waals crystals, *Scientific Reports*, **7**, (2017), 15365, https://doi.org/10.1038/s41598-017-15763-1
[10] L. Bychto, M. Malinski, Photoacoustic spectroscopy analysis of thin semiconductor samples, *Opto-Electronics Review*, **26** (2018) 217–222, https://doi.org/10.1016/j.opelre.2018.06.005
[11] Katarina Lj Djordjevic, Dragan D Markushev, Žarko M Ćojbašić, Slobodanka P Galović, Inverse problem solving in semiconductor photoacoustics by neural networks, *Inverse Problems in Science and Engineering*, **29**, 248-262, (2021), https://doi.org/10.1080/17415977.2020.1787405
[12] D. K. Markushev, D. D. Markushev, S. M. Aleksić, D. S. Pantić, S. P. Galović, D. V. Lukić and J. Ordonez-Miranda, Enhancement of the thermoelastic component of the photoacoustic signal of silicon membranes coated with a thin TiO_2 film, *Journal of Applied Physics*, **131**, 085105, (2022), https://doi.org/10.1063/5.0079902
[13] Markushev D.K., Markushev D.D., Aleksic S.M., Pantic D.S., Galovic S.P., Todorovic D.M., and J. Ordonez-Miranda, Experimental photoacoustic observation of the photogenerated excess carrier influence on the thermoelastic response of n-type silicon, *Journal of Applied Physics*, **128**, 095103 (2020), https://doi.org/10.1063/5.0015657
[14] Markushev D.K., Markushev D.D., Aleksic S.M., Pantic D.S., Galovic S.P., Todorovic D.M., and J. Ordonez-Miranda, Effects of the photogenerated excess carriers on the thermal and elastic properties of n-type silicon excited with a modulated light source: Theoretical analysis, *Journal of Applied Physics*, **126** (18), 185102 (2019), https://doi.org/10.1063/1.5100837
[15] Penghong Ci, Muhua Sun, Meenakshi Upadhyaya, Houfu Song, Lei Jin, Bo Sun, Matthew R. Jones, Joel W. Ager, Zlatan Aksamija, Junqiao Wu, Giant Isotope Effect of Thermal Conductivity in Silicon Nanowires, *Physical Review Letters*, **128** (8), (2022), https://doi.org/10.1103/PhysRevLett.128.085901
[16] Bairi Levi Rakshith, Lazarus Godson Asirvatham, Appadurai Anitha Angeline, Stephen Manova, Jefferson Raja Bose, J Perinba Selvin Raj, Omid Mahian, Somchai Wongwises, Cooling of high heat flux miniaturized electronic devices using thermal ground plane: An overview, *Renewable and Sustainable Energy Reviews*, **170**, (2022), 112956, https://doi.org/10.1016/j.rser.2022.112956
[17] Junaid Khan, Syed Abdul Momin, M. Mariatti, A review on advanced carbon-based thermal interface materials for electronic devices, *Carbon*, **168**, (2020), 65-112, https://doi.org/10.1016/j.carbon.2020.06.012

[18] Jiale Su, Xinwei Zhang, Guoping Zhou, Changfeng Xia, Wuqing Zhou and Qing'an Huang, A review: crystalline silicon membranes over sealed cavities for pressure sensors by using silicon migration technology, *Journal of Semiconductors*, **39** (7), 071005, (2018), https://doi.org/10.1088/1674-4926/39/7/071005
[19] P.G. Ullmann, C. Bretthauer, M. Schneider, U. Schmid, Stress analysis of circular membrane-type MEMS microphones with piezoelectric read-out, *Sensors and Actuators A: Physical*, **349**, (2023), 114003, https://doi.org/10.1016/j.sna.2022.114003
[20] Bagolini, A., Correale, R., Picciotto, A., Di Lorenzo, M., Scapinello, M., MEMS Membranes with Nanoscale Holes for Analytical Applications, *Membranes*, **11** (2), (2021), 74, https://doi.org/10.3390/membranes11020074
[21] Giuseppe Bertuccio, On the physical origin of the electro-mechano-acoustical analogy, *The Journal of the Acoustical Society of America*, **151**, (2022), 2066, https://doi.org/10.1121/10.0009803
[22] Eric Brandão, William D'Andrea Fonseca and Paulo Henrique Mareze, An algorithmic approach to electroacoustical analogies, *The Journal of the Acoustical Society of America*, **152**, (2022), 667, https://doi.org/10.1121/10.0012886
[23] Taha, W.M., Taha, AE.M., Thunberg, J. (2021). Modeling Physical Systems. In*: Cyber-Physical Systems: A Model-Based Approach*, Springer, Cham. https://doi.org/10.1007/978-3-030-36071-9_2
[24] D. Sundararajan, *Digital Signal Processing, An Introduction*, Springer Nature Switzerland AG (2021), https://doi.org/10.1007/978-3-030-62368-5
[25] Steven W. Smith, *The Scientist and Engineer's Guide to Digital Signal Processing*, *2nd Edition*, California Technical Publishing, (1999), https://www.dspguide.com/
[26] Slobodanka Galovic, Zlatan Soskic, Marica Popovic, Analysis of photothermal response of thin solid films by analogy with passive linear electric networks, *Thermal Science*, **13** (4), 129-142, https://doi.org/10.2298/TSCI0904129G
[27] George Ellis, Chapter 8 – Filters in Control Systems, in *Control System Design Guide (Fourth Edition)*, (2012), 165-183, https://doi.org/10.1016/B978-0-12-385920-4.00009-6
[28] Luis F. Chaparro, Aydin Akan, Chapter 12 – Introduction to the Design of Discrete Filters, in *Signals and Systems Using MATLAB (Third Edition)*, (2019), 721-802, https://doi.org/10.1016/C2017-0-00826-1
[29] Alan S. Morris, Reza Langari, Chapter 8 – Principles of data acquisition and signal processing, in *Measurement and Instrumentation (Third Edition), Theory and Application*, (2021), 211-241, https://doi.org/10.1016/B978-0-12-817141-7.00008-6
[30] Rosencwaig, A., Gersho, A., Theory of the photoacoustic effect with solids, *Journal of Applied Physics*, **47**, 64–69, (1976), https://doi.org/10.1063/1.322296
[31] Rosencwaig, A. *Photoacoustics and Photoacoustic Spectroscopy*; John Wiley & Sons: New York, NY, USA, (1980), pp. 1–309.
[32] Stephen E. Bialkowski, Nelson G.C. Astrath, Mikhail A. Proskurnin, (2019) *Photothermal Spectroscopy Methods for Chemical Analysis*, 2nd Edition (New York: John Wiley), ISBN: 978-1-119-27907-5
[33] McDonald FA, Photoacoustic, photothermal, and related techniques: a review, *Canadian Journal of Physics*, **64**, (1986), 1023-1029, https://doi.org/10.1139/p86-174
[34] McDonald F and Wetsel G, Generalized theory of the photoacoustic effect, *Journal of Applied Physics*, **49**, (1978), 2313, https://doi.org/10.1063/1.325116
[35] B.A. Boley and J.H. Weiner, *Theory of Thermal Stresses*, Wiley, New York, (1960)

[36] Roussett G., Lepoutre F., and Bertrand L., *Journal of Applied Physics*, **54**, 2383 (1983), https://doi.org/10.1063/1.332352
[37] D.D. Markushev, J. Ordonez-Miranda, M.D. Rabasovic, M. Chirtoc, D.M. Todorovic, S.E. Bialkowski, D. Korte and M. Franko, Thermal and elastic characterization of glassy carbon thin films by photoacoustic measurements, *The European Physical Journal Plus*, **132**, 33 (2017) 1-9, https://doi.org/10.1140/epjp/i2017-11307-2
[38] D. D. Markushev, J. Ordonez-Miranda, M. D. Rabasović, S. Galović, D. M. Todorović, and S. E. Bialkowski, Effect of the absorption coefficient of aluminium plates on their thermoelastic bending in photoacoustic experiments, *Journal of Applied Physics*, **117**, 245309 (2015), https://doi.org/10.1063/1.4922718
[39] Vitalyi Gusev and Mladen Franko, Editorial for the special collection on non-invasive and non-destructive methods and applications, I: Festschrift—A tribute to Andreas Mandelis, *Journal of Applied Physics*, **132**, 230401 (2022); https://doi.org/10.1063/5.0133988
[40] K. Herrmann, N.W. Pech-May, M. Retsch, Photoacoustic thermal characterization of low thermal diffusivity thin films, *Photoacoustics*, **22** (2021) 100246, https://doi.org/10.1016/j.pacs.2021.100246
[41] Alexander Melnikov, Andreas Mandelis, Akshit Soral, Claudia Zavala-Lugo, and Michal Pawlak, Quantitative Imaging of Defect Distributions in CdZnTe Wafers Using Combined Deep-Level Photothermal Spectroscopy, Photocarrier Radiometry, and Lock-In Carrierography, *ACS Appl. Electron. Mater.* 2021, **3**, 6, 2551–2563, https://doi.org/10.1021/acsaelm.1c00100
[42] M. Pawlak, Photothermal, photocarrier, and photoluminescence phenomena in semiconductors studied using spectrally resolved modulated infrared radiometry: Physics and applications editors-pick, *Journal of Applied Physics* **126**, 150902 (2019); https://doi.org/10.1063/1.5114719
[43] Jacek Zakrzewski, Karol Strzałkowski, Mohammed Boumhamdi, Agnieszka Marasek, Ali Abouais and Daniel M. Kaminski, Photothermal Determination of the Surface Treatment of $Cd_{1-x}Be_xTe$ Mixed Crystals, *Appl. Sci.* 2023, **13** (4), 2113; https://doi.org/10.3390/app13042113
[44] D. D. Markushev, M. D. Rabasović, D. M. Todorović, S. Galović, and S. E. Bialkowski, Photoacoustic signal and noise analysis for Si thin plate: Signal correction in frequency domain, *Review of Scientific Instruments*, **86**, 035110 (2015), https://doi.org/10.1063/1.4914894

Appendix I. Photothermal response and analogy with passive linear electric networks

The thermal response of the sample illuminated by modulated light source is described by the temperature distribution $T_s(z)$ within the sample (Eq. (7)), obtained by solving the dynamic part of the 1D diffusion equation of heat transport along the *z*-axes:

$$\frac{\partial^2 T_s(z,t)}{\partial z^2} = \frac{1}{D_T}\frac{\partial T_s(z,t)}{\partial t}, \tag{A1.1}$$

where $T_s(z,t) = T_{amb}(z) + T_s(z)\left(1+e^{j\omega t}\right)$, $T_{amb}(z)$ is the ambient temperature, ω is the modulation circular frequency, $D_T = k/(\rho C_V)$, k is the thermal conductivity, ρ is the density and C_V is the volumetric thermal capacity of the medium. This equation is, so called, parabolic heat conduction equation (PHCE), that is always stable, depicting heat transfer process in medium as a diffusion process. It assumes an infinite speed of heat propagation or, in other words, the zero-relaxation time $(\tau \to 0)$ of thermal processes in the medium. On the other hand, the 1D hyperbolic heat conduction equation (HHCE) along the *z*-axes [26],

$$\frac{\partial^2 T_s(z,t)}{\partial z^2} = \frac{1}{D_T}\frac{\partial T_s(z,t)}{\partial t} + \frac{\tau}{D_T}\frac{\partial^2 T_s(z,t)}{\partial t^2}, \tag{A1.2}$$

acknowledges the finite speed of heat propagation, or finite value of τ $(\tau \neq 0)$, describing the heat transfer process in medium as a wave propagation process. The Eq. (A1.2) is similar in form to the Maxwell (telegraph) equation of an electromagnetic field, which, given in the terms of voltage $u(z,t)$ between the lines has the form [26]:

$$\frac{\partial^2 u(z,t)}{\partial z^2} = rc\frac{\partial u(z,t)}{\partial t} + l_z c\frac{\partial^2 u(z,t)}{\partial t^2}, \tag{A1.3}$$

where $r = \mathrm{d}R/\mathrm{d}z$ is the distributed resistance, $c = \mathrm{d}C/\mathrm{d}z$ – the distributed capacitance and $l_Z = \mathrm{d}L/\mathrm{d}z$ – the distributed inductance of the line. An analogy between the Eq. (A1.2) and Eq. (A1.3) can be established, as an analogy between two distributed parameters systems, by introducing the following relationships: $u \leftrightarrow T$, $c \leftrightarrow \rho C_V$, $r \leftrightarrow 1/k$ and $l_Z \leftrightarrow \tau/k$.

However, the electric network which consists of the elements with lumped (not anymore distributed) parameters can be established to describe the system defined with Eq. (A1.3). Such system consists of the equivalent impedance Z_{eq} and admittance Y_{eq}, given in the forms [26]:

$$Z_{\mathrm{eq}} = Z\frac{\tanh\left(\frac{\sqrt{ZY}}{2}\right)}{\frac{\sqrt{ZY}}{2}} \text{ and } Y_{\mathrm{eq}} = Y\frac{\sinh\left(\sqrt{ZY}\right)}{\sqrt{ZY}}, \tag{A1.4}$$

where

$$Z = l_l\left(r + j\omega l_z\right) \text{ and } Y = j\omega c l_l, \tag{A1.5}$$

and l_l is the length of the line. If one wants to represent Z_{eq} and Y_{eq} with real electric elements (resistors, capacitors and coils), the Eq. (A1.4) must be simplified to:

$$Z_{\mathrm{eq}} = Z \text{ and } Y_{\mathrm{eq}} = Y, \tag{A1.6}$$

This can be done if the condition $ZY \ll 6$ is satisfied, as shown in [26].

If $\tau = 0$ is the case we are considering, the equivalent electric circuit that describes the optically induced surface temperature variations is an *RC* filter (the coil as an element is lost). The equivalent impedance Z_{eq} and the equivalent admittance Y_{eq} are given by the expressions:

$$Z_{eq} = Z = l_l r = \frac{1}{k} l_l \text{ and } Y_{eq} = Y = j\omega c l_l = j\omega\rho C_v l_l. \tag{A1.7}$$

Using the knowledge that the properties of materials in relation to heat conduction can, under certain conditions, be described as equivalent to resistance and capacitance (Eq. (A1.7)), the condition under which the TE component of the PA signal (Eq. (8)) can be described with *RC* filters is $ZY \ll 24$ (obtained following the series expansion of $\tanh\left(\sqrt{ZY}/2\right)/\left(\sqrt{ZY}/2\right)$) [26]. The condition can be written as:

$$ZY = l_l r j\omega c l_l = j\omega r c l_l^2 \ll 24, \tag{A1.8}$$

or rewritten in terms of sample properties using established analogies (sample thickness $l = l_l$) [26]:

$$j\omega\frac{1}{D_T} l^2 \ll 24. \tag{A1.9}$$

This condition in the terms of real numbers can be written as

$$\omega\frac{1}{D_T} l^2 = \left(|\sigma| l\right)^2 \ll 24, \tag{A1.10}$$

which leads to the final form of $|\sigma| l \ll 2\sqrt{6}$. Taking into account the obtained limits and series expansion, the analytical expression of the $\delta p_{\mathrm{TE}}\left(j\omega\right)_{\mathrm{s}}$ (Eq. (8)) can be simplified as:

$$\delta p_{\mathrm{TE}}\left(j\omega\right)_{\mathrm{s}} = 3\pi \frac{I_0 \gamma_{\mathrm{g}} p_0 \alpha_T R^4}{8 m^2 k V_0}\left[\frac{1}{1+\left(j\omega/\omega_{\mathrm{TE}}\right)}\right], \tag{A1.11}$$

where

$$A_{\mathrm{TE}}\left(j\omega\right)_{\mathrm{s}} = \left|\delta p_{\mathrm{TE}}\left(j\omega\right)_{\mathrm{s}}\right| \propto \frac{1}{\sqrt{1+\left(\omega/\omega_{\mathrm{TE}}\right)^2}}, \text{ and } \varphi = -\arctan\left(\frac{\omega}{\omega_{\mathrm{TE}}}\right). \tag{A1.12}$$

Here $\omega_{\mathrm{TE}} = D_T / \left(l/2m\right)^2$, and $\sqrt{2} \le m < \sqrt{6}$, depending on number of terms in series expansion.

Appendix II. The cleaning of experimental signal from the influence of the measuring chain

The measuring chain of photoacoustics consists of many devices with associated electronics that measure not only the desired signal but also control the conditions of the experiment, especially the sources of excitation. All these devices, in addition to their good features, carry with them (as electronic devices) plenty of bad features that are reflected in different types of noise and strong signal deviations in the entire frequency domain of interest for our research [44].

In our case, the microphone as a detector, with its associated electronics, introduces the most interference and affects the shape of the measured signal in the entire range of modulation frequencies f from 20 Hz to 20 kHz. In the low-frequency range ($f < 10^3$ Hz), the microphone and the lock-in, which is emulated by the computer's sound card, act like two cascaded high-pass RC filters, decreasing the measured signal more and more as we move towards lower frequencies. In a mathematical sense, their influence can be described by a transfer function $H_{\mathrm{e}}\left(j\omega\right)$ of the first order having the form:

$$H_{\mathrm{e}}\left(j\omega\right) = -\frac{\left(\frac{\omega}{\omega_1}\right)}{\left(1+j\frac{\omega}{\omega_1}\right)} \times \frac{\left(\frac{\omega}{\omega_2}\right)}{\left(1+j\frac{\omega}{\omega_2}\right)}, \tag{A2.1}$$

where $\omega = 2\pi f$, $\omega_1 = 2\pi f_1$, where f_1 is the microphone cut-off frequency, and $\omega_2 = 2\pi f_2$, where f_2 is the lock-in (sound card) cut-off frequency. In the high-frequency range, the microphone acts like two second-order high-pass RC filters, altering the measured signal in the form of peaks (resonances) more and more as we move toward higher frequencies. In a mathematical sense, microphone influence (acoustic response) can be described by a transfer function $H_{\mathrm{a}}\left(j\omega\right)$ of the second order having the form [44]:

$$H_{\mathrm{a}}(j\omega)=\frac{1}{1-\left(\frac{\omega}{\omega_3}\right)^2+j\delta_3\frac{\omega}{\omega_3}}+\frac{1}{1-\left(\frac{\omega}{\omega_4}\right)^2+j\delta_4\frac{\omega}{\omega_4}}, \tag{A.2.2}$$

Here $\omega_3=2\pi f_3$, $\omega_4=2\pi f_4$, where f_3 and f_4 are the characteristic cut-off frequencies of the first and second peaks of the microphone, while δ_3 and δ_4 are their corresponding dumping factors.

The measured photoacoustic signal $S(j\omega)_{\mathrm{s}}$ is the product of the "real" photoacoustic signal $\delta p_{\mathrm{total}}(j\omega)_{\mathrm{s}}$ originating from the sample, multiplied by the aforementioned effects of $H_{\mathrm{e}}(j\omega)$ and $H_{\mathrm{a}}(j\omega)$ in the entire frequency domain [44]:

$$S(j\omega)_{\mathrm{s}}=\delta p(j\omega)_{\mathrm{s}}H_{\mathrm{e}}(j\omega)H_{\mathrm{a}}(j\omega). \tag{A2.3}$$

The basic idea of cleaning the measured signal is to recognize all the mentioned cut-off frequencies of the microphone and lock-in (sound card), e.g. by fitting the $S(j\omega)_{\mathrm{s}}$. In this way, $H_{\mathrm{e}}(j\omega)$ and $H_{\mathrm{a}}(j\omega)$ can be fully recognized and removed from the measured signal, leaving only the "real" signal $\delta p_{\mathrm{total}}(j\omega)_{\mathrm{s}}$ that carries information about the illuminated sample. The “real” signal now can be the subject of fitting based on, for example, the theory of composite piston, searching for the signal components, especially thermoelastic one.